Supporting Information

Volman et al. 10.1073/pnas.1112066108

SI Materials and Methods

Computational Model of Cortical Trauma. ***Computational model of cortical network.*** The dynamics of both pyramidal (PY) neurons and interneurons (INs) are described with the one-compartment, two-variable Morris–Lecar model, which is modified to account for the correct membrane potential profile of neuronal spikes (1, 2). In addition, a spike frequency adaptation mechanism (2) was incorporated into the model of PY neurons to account for the activity-dependent adaptation displayed by these neurons. The equations that govern the neuronal dynamics are (parameters listed in Table S1) (Eqs. **S1–S6**)

$$C\frac{dV}{dt} = -g_{Na}m_\infty(V-E_{Na}) - g_K\omega(V)(V-E_K) - g_L(V-E_L) - I_{ad} - I_{syn} - I_{aff}, \quad \text{[S1]}$$

$$\frac{d\omega}{dt} = \phi\cdot(\omega_\infty(V)-\omega)\cosh((V-V_3)/2V_4), \quad \text{[S2]}$$

$$m_\infty(V) = 0.5\cdot(1+\tanh((V-V_1)/V_2)), \quad \text{[S3]}$$

$$\omega_\infty(V) = 0.5\cdot(1+\tanh((V-V_3)/V_4)), \quad \text{[S4]}$$

$$I_{ad}(t) = g_{ad}z(V-E_K), \text{ and} \quad \text{[S5]}$$

$$\frac{dz}{dt} = \alpha\left[\frac{1}{(1+\exp((\beta-V)/\gamma))} - z\right]. \quad \text{[S6]}$$

Eqs. **S1–S4** are a one-compartment, two-variable Morris–Lecar model of neuronal dynamics (1), which is modified to account for correct voltage of spike generation in central neurons (2). Eqs. **S5** and **S6** are for the adaptation current (2) that is added only to the dynamics of model PY neurons.

Synaptic currents at PY–PY synapses had both AMPA and NMDA components, with both AMPA and NMDA conductances attenuated by synaptic depression as described below. Inhibitory synaptic currents did not incorporate synaptic depression.

Synaptic transmission was modeled as a deterministic process in which the dynamics of AMPA and $GABA_A$ synaptic conductances were described by the following generic equation, with τ_D being the characteristic time of postsynaptic current decay (Eq. **S7**):

$$\frac{dg_{AMPA,GABA}}{dt} = -\frac{g_{AMPA,GABA}}{\tau_D} + G_{X\leftarrow PY,X\leftarrow IN}D\delta(t-t_{spike}). \quad \text{[S7]}$$

The value of maximal synaptic conductance, G, depended on the pre- and postsynaptic neurons. Thus, $G_{PY\leftarrow PY}$ (maximal synaptic conductance from PY to PY) was different from $G_{IN\leftarrow PY}$ (maximal synaptic conductance from PY to inhibitory IN). The values of these conductances are given in Table S1.

Temporal dynamics of NMDA conductance were modeled as a difference of fast (g_F) and slow (g_S) exponentially decaying components (Eqs. **S8** and **S9**):

$$g_{NMDA}(t) = \frac{g_S(t)-g_F(t)}{1+0.33[\mathrm{Mg}]\exp(-0.06\mathrm{V})} \text{ and} \quad \text{[S8]}$$

$$\frac{dg_{F,S}}{dt} = -\frac{g_{F,S}}{\tau_{F,S}} + G_{NMDA}D\delta(t-t_{spike}). \quad \text{[S9]}$$

The parameter D accounted for the efficacy of synaptic transmission. For GABAergic synapses, this parameter was held fixed ($D = 1$). For excitatory AMPA and NMDA synapses, it evolved according to the following equation, with U representing the strength of synaptic short-term depression (3) (Eq. **S10**):

$$\frac{dD}{dt} = \frac{1-D}{\tau_R} - U\delta(t-t_{spike}). \quad \text{[S10]}$$

Unless otherwise specified, all synaptic parameters were the same as the ones reported in Table S1. The different synaptic currents were described by the following equations (Eqs. **S11–S13**):

$$I_{AMPA}(t) = g_{AMPA}(t)(V-E_{AMPA}), \quad \text{[S11]}$$

$$I_{NMDA}(t) = g_{NMDA}(t)(V-E_{NMDA}), \text{ and} \quad \text{[S12]}$$

$$I_{GABA}(t) = g_{GABA}(t)(V-E_{GABA}). \quad \text{[S13]}$$

In addition to synaptic currents from their peers inside the network, each model neuron was also stimulated by inputs from other cortical areas. For each neuron, this stimulation was modeled as an independent and uncorrelated Poisson process (100 Hz) that stimulated the canonic AMPA conductance g_{EX} at times t_{EX} (Eqs. **S14** and **S15**):

$$\frac{dg_{EX}}{dt} = -\frac{g_{EX}}{\tau_{EX}} + G_{EX}\delta(t-t_{EX}) \text{ and} \quad \text{[S14]}$$

$$I_{aff}(t) = g_{EX}(t)(V-E_{AMPA}). \quad \text{[S15]}$$

Synaptic strength parameters in the baseline version of this computational model (before action of homeostatic plasticity) were constrained by the firing characteristics of cortical neurons in intact cortex. There were four specific requirements on model neurons. (*i*) Both PYs and INs fire asynchronously in the baseline model of intact cortex. (*ii*) Synaptic interactions contribute significantly to neuronal firing. (*iii*) PYs display spike frequency adaptation. (*iv*) The mean rate of PY firing is ∼5 Hz, and the mean rate of IN firing is ∼10 Hz. As shown in the work by Houweling et al. (4), an asynchronous state can be obtained only if the average recurrent synaptic conductance is constrained to be smaller than the synaptic conductance that conveys afferent excitation to a model neuron. That is, synaptic conductance has to satisfy $G_{PY\leftarrow PY} < G_{PY\leftarrow EX}$ and $G_{IN\leftarrow PY} < G_{IN\leftarrow EX}$. With these considerations in mind, parameters were similar to the parameters reported in Table S1.

In this work, we considered 2D cortical networks of 80 × 80 model neurons, of which 80% (5,120 neurons) were excitatory; the remaining 20% (1,280 neurons) were inhibitory. Each model neuron could establish, with probability $p_c = 0.6$, a unidirectional synaptic connection with any other model neurons found within its footprint (10 × 10 neurons). In some simulations, we scaled the network size from 80 × 80 to 160 × 160 neurons (leaving all other parameters the same) to check the robustness of our observations. The effect of self-synapses (autapses) was not addressed in the present study. To account for possible variations in intrinsic excitability of cortical neurons, the actual value of leak conductance, g_L, was drawn from Gaussian distribution centered around the mean $\widetilde{g}_L$ ($\sigma_g = 0.08$) and truncated at $[0.95\widetilde{g}_L, 1.05\widetilde{g}_L]$.

Deafferentation of model cortical network. Cortical deafferentation was modeled here as a two-parameter scenario (f_D and r_D) in which either the fraction of deafferented cells, f_D, or the drop in the rate of external stimulation, r_D, could be varied. Thus, a pair ($f_D = 0.4$, $r_D = 0.1$) designates the scenario in which 40% of model neurons had the rate of their external stimulation reduced to 10% of its value in intact cortex model (100 Hz). In the case of random deafferentation, the spatial pattern of deafferentation was determined by random selection of the corresponding number of model neurons.

Homeostatic regulation of synaptic conductances. Experimental evidence (5, 6) and computational models (4, 7, 8) have shown that homeostatic plasticity (HSP) plays an important role in the reorganization of cortical networks' activity after deafferentation. Homeostatic plasticity is a multifaceted process that encompasses activity-dependent change in synaptic conductance (9) as well as changes in intrinsic excitability (10) or modulation of synaptic transmitter release probability (11).

To avoid conflating the effects of different factors, we concentrated on the homeostatic regulation of synaptic conductances and used a simple rule of HSP cast in the following equations (4) (Eqs. **S16** and **S17**):

$$G_{PY\leftarrow PY} = G_{PY\leftarrow PY} + \alpha_{HSP}(v_0 - \bar{v})G_{PY\leftarrow PY} \text{ and} \qquad \textbf{[S16]}$$

$$G_{PY\leftarrow IN} = G_{PY\leftarrow IN} - 0.5\cdot\alpha_{HSP}(v_0 - \bar{v})G_{PY\leftarrow IN}. \qquad \textbf{[S17]}$$

Because homeostatic regulation of synaptic and intrinsic conductances occurs on the time scale of hours and days, computational modeling of these processes becomes intractable. In Eqs. **S16** and **S17**, the parameter α_{HSP} is the rate of homeostatic update, and $v_0 = 5$ Hz is the preset target rate of PY neurons firing (similar to the network-averaged firing rate of model PY neurons in the baseline model of healthy cortical network). Similar to the scheme used in refs. 4 and 7, at the end of a 4-s window, the network-averaged firing rate of model pyramidal neurons, $\bar{v}$, is computed, and then, Eqs. **S16** and **S17** are applied to model synapses. Thus, Eqs. **S16** and **S17** constitute a discrete approximation of homeostatic regulation; however, by increasing the time window (from 4 to 8 s), we have verified that our conclusions regarding the role of trauma pattern in epileptogenesis are robust with respect to the choice of specific averaging time. Experimental data (9) suggest that homeostatic changes in synaptic conductances occur within the range of 100%. Therefore, in our model, a hard bound on the maximal value of synaptic conductance was imposed, preventing it from increasing beyond 100% of the initial value. Simultaneously, a minimal value of zero was required for synaptic conductance to prevent the possibility of negative values after down-regulation by HSP. Although recent evidence indicates that excitatory synapses onto inhibitory interneurons are also subject to homeostatic regulation (12), we assumed that only the synapses on PY neurons are modified after trauma.

Detection of network bursting events. We used here the following algorithm to detect the events of intense collective activity (which we henceforth term network bursting events). First, the time of recording is partitioned into nonoverlapping bins of 100 ms each. Binned spike count for each model neuron is obtained. As a rule of thumb, a bursting event occurs in time bin T_{burst} if at least $N_{BT} = f_{BT}N$ of recorded model neurons fired action potentials during this time bin, with an average rate of firing greater than v_{BT}. This operational definition is constrained by the minimal fraction of active neurons, f_{BT}, that define the bursting events and by the minimal intraburst firing rate, v_{BT}, of these active neurons. In most of our analyses, we set $f_{BT} = 0.5$ and $v_{BT} = 15$ Hz. In the analysis that aimed to address the stochastic invasion of bursting events into the deafferented cortex, the minimal fraction of active neurons was reduced to $f_{BT} = 0.1$. In general, reduction of f_{BT} led to the detection of more spatially localized bursting events. However, higher v_{BT} led to the detection of only those events during which the neuronal activity was significantly intense.

Because it is computationally intractable to analyze the activity of an entire network of 6,400 neurons, we sampled the activity of a subset of neurons, using this sample to estimate the rate of bursting events in the network. In the case of a randomly deafferented network, the sampling region was a square block (usually 20 × 20 model neurons) cocentered with the center of the 2D network. In the case of a block-deafferented network, the sampling region was composed of five parallel adjacent lines (resulting in a total of 400 model neurons). These sampling considerations were based on the realization that spatially random deafferentation should result in activity roughly symmetric with respect to the center of the lattice, whereas in the block-deafferented case, the activity is likely to propagate from intact into deafferented regions. Changing the sampling rules (i.e., performing center-symmetric sampling for block-deafferented cases) did not qualitatively change our conclusions regarding the difference between the random and spatially structured deafferentation.

Correlated inputs. In a preliminary set of simulations, we tested the effect that the correlation between afferent inputs would have on the reorganization of electrical activity in posttraumatic cortical network. We followed the method used in the work by Rudolph and Destexhe (13) to generate correlation between afferent inputs to different model neurons. Specifically, at each time step ($dt = 0.1$ ms), N_0 Poisson-distributed events were generated, with $N_0 = N - (N-1)\sqrt{c}$. These N_0 events were then randomly distributed across $n = 6{,}400$ model neurons. The correlation between the activities of different afferents follows, because the correlation parameter, c, introduces instantaneous redundancy in synaptic activity ($N_0 \leq N$).

Effects of Spike Frequency Adaptation on the Activity of Model PY Neurons. Our primary focus was to understand the influence that the network structure and spatial organization of trauma pattern might have on the genesis of epileptic-like activity after trauma. However, before studying the network effects, it was important to understand how cell-intrinsic parameters can affect its dynamics. Here, we consider the effects of the spike frequency adaptation (the hyperpolarizing conductance).

In our model of cortical neuronal network, the spike-generating dynamics of both excitatory PY neurons and inhibitory INs were described by a variant of the Morris–Lecar model that was slightly modified to account for correct membrane voltages of spike generation (1, 2). Spiking activity of real excitatory PY neurons in the cortex is subject to adaptation. To account for this effect, we added a phenomenological spike frequency adaptation hyperpolarizing conductance to the dynamical equation of excitatory neurons.

To show how such spike frequency adaptation modifies the firing properties of excitatory model neurons, we considered the response of isolated model neurons (not connected to the network) driven by afferent excitation for different strengths of adaptation conductance. Fig. S1 shows that increasing adaptation conductance always acted to decrease the firing rate of a model neuron; this effect of spike frequency adaptation is stronger for higher values of afferent excitatory synaptic conductance, G_{EX} (which led to higher neuronal firing rates). Both the mean (Fig. S1 *Center*) and SD (Fig. S1 *Right*) of subthreshold membrane potential were lower for stronger adaptation.

Dissipation of Network Bursts by Asynchronous Activity of Intact Neurons. To assess the destructive effects that the asynchronous activity might have on the nucleation and propagation of seizure-like network bursts, we computed the rate of bursts (using the same criteria for burst detection as described in the text) for different sizes of sampling regions. If intact asynchronous activity acts to dissipate the propagation of bursts through the network, we would expect to see a negative correlation between the sampling block size and rate of bursts (i.e., lower apparent rate of bursts for larger samples). Moreover, the dependence of burst rate on the sample size is expected to be stronger for milder deafferentation (smaller values of f_D).

Fig. S2*A* shows the results of this analysis. The sampling region here was a block (of increasing size) symmetric relative to the center of the 2D square lattice defined by model neurons. The apparent rate of network bursts indeed decreases with increasing sample size; this effect depends on the severity of deafferentation (as captured by f_D). For a given drop r_D in afferent excitation rate, milder deafferentation (smaller f_D) leads to a steeper relation between the burst rate and sampling block size.

As another measure of burst dissipation, we computed the pair cross-covariance between activities of deafferented neurons, plotting these results vs. the distance D_{ij} (on lattice) between the neurons. If burst propagation is hampered by the asynchronous activity of intact neurons, we would expect the cross-covariance to decrease with the increasing distance between the neurons. As before, the steepness of this relation is expected to depend on the drop r_D in afferent excitation rate as well as on the fraction of deafferented neurons f_D, with greater r_D leading to a faster decay of cross-covariance.

To compute the cross-covariance, each neuron in the binary spike time series $\{t_i\}$ was convolved with the Gaussian function ($\mu_G = 0$, $\sigma_G = 1.5$) to obtain smooth presentation of neuronal spiking activity, $\{S_i\}$. The cross-covariance C_{ij} was then estimated as (Eq. **S18**)

$$C_{ij} = \frac{\left\langle \left(S_i - \mu_{S_i}\right)\left(S_j - \mu_{S_j}\right)\right\rangle}{\sigma_{S_i}\sigma_{S_j}}, \qquad \textbf{[S18]}$$

where μ_{S_i} and σ_{S_i} are the mean and SD of S_i.

Applying the above algorithm, a set of (C_{ij}, D_{ij}) pairs is obtained for all pairs of neurons under consideration. Data presented in Fig. S2*B* were generated by first distributing the pair distances in bins, each of 1.5 lattice constants width, and then computing the mean cross-covariance for all (C_{ij}, D_{ij}) pairs in the given distance bin. The Y values in Fig. S2*B* are, therefore, an estimate of pair cross-covariance for neuronal pairs separated by the distance $D \pm 1.5$ lattice constants.

Fig. S2*B* shows that cross-covariance of electrical activity is negatively correlated with the lattice distance between the neurons, with lower values attained for neurons that are farther apart. As expected, cross-covariance is lower for weaker drops in afferent excitation rate (higher values of r_D) and milder deafferentation (smaller values of f_D), lending additional support to the hypothesis of burst dissipation by asynchronous activity. Thus, we conclude that bursts that are nucleated by the network are dissipated as they propagate through the intact tissue. An immediate corollary is that the spatial organization of intact vs. deafferented regions is expected to critically affect the chances to observe epileptic seizures in posttraumatic cortical network.

Posttraumatic Reorganization of Activity in Severely Traumatized Network Depends on the Spatial Distribution of Intact Neurons. Results for severely deafferented network (Fig. 2*F*) indicate that posttraumatic reorganization of electrical activity might depend on the spatial distribution of intact neurons. We set out to elaborate on the network mechanisms of this relation. Results presented below were obtained for simulations of very severe deafferentation scenarios in which only a relatively small number of model neurons, N_i, was left intact (we considered the cases of $N_i = 100$ and $N_i = 400$ intact neurons of 6,400 neurons total). In different simulations, the remaining intact neurons were uniformly distributed within a square of different side length, l_i, that was varied between experiments, thus resulting in networks with different spatial density of intact neurons, $\rho_i = N_i/l_i^2$ (Fig. S3*A*).

In Fig. S3*C*, the dependence of burst rate on the spatial density (ρ_i) of intact neurons is shown. The rate with which bursting events could be nucleated in the network depended on the spatial density of intact neurons, with low spatial density (more diffuse distribution of intact neurons) resulting in low burst rates. Both the mean firing rate of the remaining intact neurons (Fig. S3*E*) and fluctuations in collective activity over time (Fig. S3*B*) strongly depended on the spatial distribution of intact neurons. More compact distribution of intact neurons (larger ρ_i) required less HSP to bring the network back to the steady state (Fig. S3*D*). This finding is consistent with the notion that a sufficiently compact distribution of intact neurons promotes the formation of intact recurrent circuits. In the absence of strong asynchronous activity in the surrounding deafferented neurons, these intact recurrent circuits can amplify the afferent excitation to the point of burst nucleation. Consistent with this explanation, when the number (N_i) of remaining intact neurons was increased, the rate of network bursts slightly increased for the same spatial density of intact neurons (Fig. 3 *C*–*E*, black squares vs. red circles).

These results show that, in the case of very severe deafferentation, when most of the neurons in the network are deprived of afferent excitation, a small number of remaining intact neurons can strongly affect the propensity of a network to generate seizure-like activity; this propensity strongly depends on the spatial density of intact neurons. This conclusion offers a testable hypothesis of the variability in the incidence of trauma-induced epilepsy, which should be higher when relatively intact groups of neurons are embedded into traumatized brain area.

1. Morris C, Lecar H (1981) Voltage oscillations in the barnacle giant muscle fiber. *Biophys J* 35:193–213.
2. Prescott SA, Ratté S, De Koninck Y, Sejnowski TJ (2006) Nonlinear interaction between shunting and adaptation controls a switch between integration and coincidence detection in pyramidal neurons. *J Neurosci* 26:9084–9097.
3. Tsodyks MV, Markram H (1997) The neural code between neocortical pyramidal neurons depends on neurotransmitter release probability. *Proc Natl Acad Sci USA* 94:719–723.
4. Houweling AR, Bazhenov M, Timofeev I, Steriade M, Sejnowski TJ (2005) Homeostatic synaptic plasticity can explain post-traumatic epileptogenesis in chronically isolated neocortex. *Cereb Cortex* 15:834–845.
5. Avramescu S, Timofeev I (2008) Synaptic strength modulation after cortical trauma: A role in epileptogenesis. *J Neurosci* 28:6760–6772.
6. Timofeev I, Bazhenov M, Avramescu S, Nita DA (2010) Posttraumatic epilepsy: The roles of synaptic plasticity. *Neuroscientist* 16:19–27.

7. Fröhlich F, Bazhenov M, Sejnowski TJ (2008) Pathological effect of homeostatic synaptic scaling on network dynamics in diseases of the cortex. *J Neurosci* 28: 1709–1720.
8. Savin C, Triesch J, Meyer-Hermann M (2009) Epileptogenesis due to glia-mediated synaptic scaling. *J R Soc Interface* 6:655–668.
9. Turrigiano GG, Leslie KR, Desai NS, Rutherford LC, Nelson SB (1998) Activity-dependent scaling of quantal amplitude in neocortical neurons. *Nature* 391:892–896.
10. Echegoyen J, Neu A, Graber KD, Soltesz I (2007) Homeostatic plasticity studied using in vivo hippocampal activity-blockade: Synaptic scaling, intrinsic plasticity and age-dependence. *PLoS One* 2:e700.
11. Murthy VN, Schikorski T, Stevens CF, Zhu Y (2001) Inactivity produces increases in neurotransmitter release and synapse size. *Neuron* 32:673–682.
12. Chang MC, et al. (2010) Narp regulates homeostatic scaling of excitatory synapses on parvalbumin-expressing interneurons. *Nat Neurosci* 13:1090–1097.
13. Rudolph M, Destexhe A (2001) Correlation detection and resonance in neural systems with distributed noise sources. *Phys Rev Lett* 86:3662–3665.

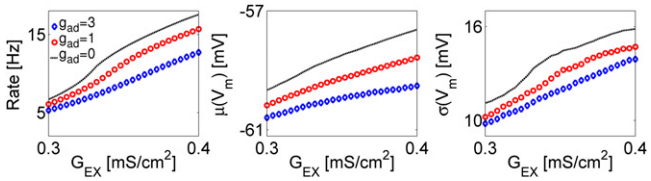

Fig. S1. Effects of spike frequency adaptation on the activity in model pyramidal neurons. (*Left*) Average firing rate of pyramidal neuron not connected to the network vs. the strength of afferent synaptic conductance, G_{EX}. Blue diamonds, g_{ad} = 3 mS/cm^2; red circles, g_{ad} = 1 mS/cm^2; dashed line, g_{ad} = 0 mS/cm^2 (as used in modeling of inhibitory interneuron). (*Center*) Average subthreshold membrane potential vs. the strength of afferent synaptic conductance, G_{EX}, over model neurons and over time. Symbols are the same as in *Left*. (*Right*) Average SD of neuronal membrane potential vs. the strength of afferent synaptic conductance, G_{EX}, over model neurons. Symbols are the same as in *Left*.

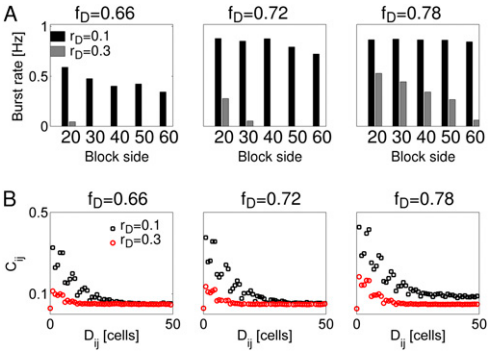

Fig. S2. Dissipation of network burst by asynchronous activity of intact neurons. (*A*) Apparent burst rate vs. the size of the sampling region (parameterized here as the side of the sampling block) for different scenarios of deafferentation: f_D = 0.66 (*Left*), f_D = 0.72 (*Center*), and f_D = 0.78 (*Right*). In all subpanels, black bars denote the case r_D = 0.1, and gray bars denote the case r_D = 0.3. (*B*) Averaged (over pairs) cross-covariance C_{ij} of neuronal activities vs. the averaged distance D_{ij} between neurons for different scenarios of deafferentation: f_D = 0.66 (*Left*), f_D = 0.72 (*Center*), and f_D = 0.78 (*Right*). In all subpanels, black squares denote the case r_D = 0.1, and red circles denote the case r_D = 0.3.

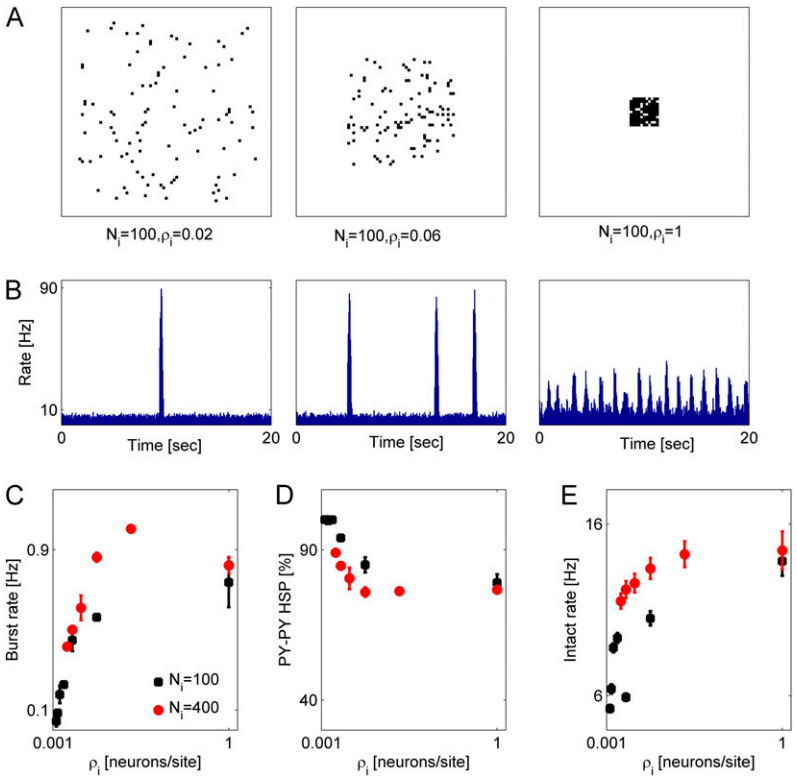

Fig. S3. Spatial density of intact neurons determines the reorganization of electrical activity after nearly complete deafferentation. (*A*) Distributions of intact neurons (black dots): N_i = 100 and ρ_i = 0.02 (*Left*), N_i = 100 and ρ_i = 0.06 (*Center*), and N_i = 100 and ρ_i = 1 (*Right*). (*B*) Temporal variations in network-averaged firing rate of intact neurons. Different panels are the same as in *A*. (*C*) Burst rate vs. the density of intact neurons. Black squares, N_i = 100; red circles, N_i = 400. Data points are mean ± SEM (n = 5). (*D*) Synaptic scaling factor (PY–PY) plotted vs. the density of intact neurons. Symbols are same as in *C*. Data points are mean ± SEM (n = 5). (*E*) Network averaged firing rate of intact neurons vs. their spatial density. Symbols are same as in *C*. Data points are mean ± SEM (n = 5).

Table S1. Values of biophysical parameters used in modeling of cortical network

Parameter	Value	Parameter	Value	Parameter	Value
V_1	−1.2 mV	E_K	−100 mV	τ_F	2 ms
V_2	23 mV	E_L	−70 mV	τ_S	80 ms
V_3	−2 mV	α	5.10^{-3} ms^{-1}	τ_R	800 ms
V_4	21 mV	β	0 mV	τ_{EX}	5 ms
C	1 μF/cm^2	γ	5 mV	U	0.07
ϕ	0.15	$G_{PY \leftarrow PY}$	74.4 μS/cm^2	[Mg]	0.8
g_{Na}	10 mS/cm^2	$G_{IN \leftarrow PY}$	89.28 μS/cm^2	E_{AMPA}	0 mV
g_K	10 mS/cm^2	$G_{PY \leftarrow IN}$	372 μS/cm^2	E_{NMDA}	0 mV
$\tilde{g}_L$	1.3 mS/cm^2	$G_{IN \leftarrow IN}$	74.4 μS/cm^2	E_{GABA}	−70 mV
σ_g	0.08 mS/cm^2	G_{NMDA}	8.928 μS/cm^2	P_C	0.6
g_{ad}	3 mS/cm^2	G_{EX}	300 μS/cm^2	α_{HSP}	0.01
E_{Na}	50 mV	τ_D	5 ms	v_0	5 Hz